08,04

On the possibility of incorporation of the iron impurity into A sites in $SrTiO_3$

© I.A. Sluchinskaya, A.I. Lebedev

Physics Department, M.V. Lomonosov Moscow State University,
Moscow, Russia

E-mail: swan@scon155.phys.msu.ru

Received November 12, 2021
Revised November 12, 2021
Accepted November 13, 2021

The local environment and oxidation state of the Fe impurity in strontium titanate are studied using XAFS spectroscopy. The influence of annealing temperature and deviation from stoichiometry on the possibility of incorporation of the impurity into the A and B sites of the perovskite structure is studied. The results obtained from the X-ray diffraction, XANES spectra, and EXAFS spectra suggest that at high annealing temperature the iron atoms, at least partially (up to 30%), enter the A sites in $SrTiO_3$. The obtained results agree with results of first-principles calculations, according to which the iron at the A site exhibits strong off-centering (the displacement of $\sim$1 Å), similar to that previously established in $SrTiO_3$ samples doped with Mn and Co.

Keywords: strontium titanate, iron, doping, XAFS, off-center atoms.

DOI: 10.21883/PSS.2022.03.53189.242

1. Introduction

The search for new multiferroics — multifunctional materials that open up new possibilities for modern electronics and spintronics — is currently an actual problem. In particular, a part of this problem concerns the search for new magnetic off-center impurities, doping with which can induce magnetoelectric interaction of their dipole and magnetic moments.

Oxides with the perovskite structure with a general formula ABO_3 have long been a subject of intensive research due to their unique properties — from ferroelectricity, piezoelectricity to colossal magnetoresistance and multiferroicity [1]. Among these oxides, strontium titanate $SrTiO_3$ is an important material whose electrical, optical, thermoelectric, and superconducting properties can be (or are already) used in various electronic and other devices [2–7]. The photocatalytic and sensory properties of doped $SrTiO_3$ are also of interest [8–10].

To obtain multiferroic properties, the crystal must simultaneously contain magnetic and dipole moments. Doping of $SrTiO_3$ with magnetic impurities of transition 3d elements enables to create magnetic moments and thereby to expand the functionality of this material by controlling it with a magnetic field. However, the position of the impurity atoms in a crystal and their local environment can significantly influence their magnetic properties. In addition, 3d elements are characterized by the possibility of their existence in several oxidation states, which depend on the position and local environment of these atoms, as well as on the presence of other donors and acceptors in the samples. Therefore, when studying such doped samples, it is necessary to study the local environment of the 3d elements.

To create dipole moments, one can try to use the idea of an off-center impurity. Off-centering is possible if a substitutional impurity enters the A site of the perovskite structure since the ionic radii of all 3d elements are much smaller than that of strontium. In this work, we analyze the possibility of Fe to enter the A site and to displace into an off-center position.

Strontium titanate doped with 3d elements has been studied since the 1960s. For a long time, it was believed that 3d elements in $SrTiO_3$ replace only Ti atoms due to the closeness of their ionic radii. The first results indicating the possibility of incorporation of 3d elements into the A site were obtained for the manganese impurity. These studies began with the discovery of unusual relaxations of the dielectric constant in $SrTiO_3$(Mn) samples [11,12]. The study of the conditions for the appearance of these relaxations first led to the assumption [13] and then to a direct proof, using the EXAFS spectroscopy, of the incorporation of manganese into the A site [14–18]. The technological conditions for this were a deviation from stoichiometry toward titanium and a high annealing temperature [13–17]. Heat treatment in a reducing atmosphere also promoted the incorporation of manganese into the A sites [17,18]. The interest to Mn-doped strontium titanate was stimulated by publications that revealed the appearance of multiferroic properties in it [19,20].

Somewhat later, using a similar approach to the synthesis of samples and the EXAFS spectroscopy technique, we prepared and studied $SrTiO_3$ samples with an off-center cobalt impurity [21,22].

Our interest to the samples doped with Fe is caused by the fact that dielectric measurements on ceramic $SrTiO_3$(Fe) samples with an intentionally created strontium

deficiency [23] revealed similar relaxation phenomena as in samples doped with off-center Mn and Co impurities. This could indicate the appearance of off-center iron atoms.

A large number of papers have been devoted to studies of iron-doped strontium titanate. It was believed that these samples are solid solutions between strontium ferrite $SrFeO_3$ and strontium titanate $SrTiO_3$, that is, the substitution occurs at the B site. Due to the difference in the oxidation states of titanium ions (Ti^{4+}) and a part of Fe ions that are in the Fe^{3+} state, the oxygen vacancies are usually present in these samples to maintain their electrical neutrality. This doping feature and the presence of iron atoms in two oxidation states (Fe^{4+} and Fe^{3+}) in samples synthesized in air results in a mixed (electronic and ionic) conductivity, which is important for the development of solid electrolytes, fuel cells, electrochemical oxygen sensors, and catalysts [24]. The study of the photochromic effect in iron-doped strontium titanate [25] and consequent finding ways to control this effect using an electric field [26] made this material a candidate for its use in resistive random access memory (ReRAM) devices.

The $SrTiO_3$(Fe) samples were studied in detail by XAFS spectroscopy. In Refs. [26,27], using XAFS spectroscopy, EPR, Raman scattering, and theoretical calculations, the ratio of the number of iron atoms in the +4 and +3 oxidation states as well as the ratio of the number of isolated Fe^{3+} ions and their complexes with the nearest oxygen vacancies were estimated in samples prepared under various conditions. In these papers, the interatomic distances in the local environment of Fe atoms were also determined. A slight increase in the Debye–Waller factor for the Fe^{4+} ion was explained by the Jahn–Teller effect, which was later confirmed by *ab initio* calculations [28]. An analysis of the X-ray absorption near-edge structure (XANES) in spectra of thin $SrTiO_3$(Fe) films prepared by pulsed laser deposition [29] in the vicinity of the Fe L-edge made it possible to establish that iron in these samples is in a mixture of +2 and +3 oxidation states. Annealing the films in vacuum resulted in an increase in the Fe^{2+}/Fe^{3+} ratio. The contrast between the results obtained for bulk samples and thin films was explained by a specific defect structure of thin films caused by their preparation under nonequilibrium conditions.

To check the possibility of the incorporation of Fe impurities into the A sites of strontium titanate, we used the same synthesis conditions as were used before in our studies of off-center Mn and Co impurities in $SrTiO_3$. The obtained samples were studied by XAFS spectroscopy. The experimental results were analyzed taking into account the results of first-principles calculations, in which theoretical models of impurity centers we could meet in the experiment according to the literature data were constructed.

2. Experimental and calculation techniques

$SrTiO_3$ samples doped with Fe with an impurity concentration of 2–3% and different deviation from stoichiometry were prepared by solid-phase synthesis. The starting components were $SrCO_3$, nanocrystalline TiO_2 obtained by hydrolysis of tetrapropylorthotitanate and dried at 500°C, and Fe_2O_3. The components were weighed in the required proportions, ground in acetone and annealed in alumina crucibles in air at 1100°C for 8 hours. The resulting powders were ground and annealed again under the same conditions. Several samples were additionally annealed in air at 1500°C for 2 hours. To incorporate impurities into the A or B sites of the perovskite structure, the composition of the samples was deliberately deviated from stoichiometry, respectively, toward excess titanium or strontium.

X-ray absorption spectra in the regions of extended fine structure (EXAFS) and near-edge structure (XANES) were recorded by detecting X-ray fluorescence at the Fe K-edge (7.112 keV) at 300 K at the KMC-2 station of the BESSY synchrotron radiation source (electron energy 1.7 GeV, maximum beam current 290 mA). The incident radiation was monochromatized with a (111)-oriented $Si_{1-x}Ge_x$ double-crystal monochromator. The intensity of this radiation (I_0) was measured using an ionization chamber. The fluorescence intensity I_f was measured with a RÖNTEC silicon drift detector operating in energy dispersive mode. The powders were rubbed into the surface of adhesive tape, which was then folded to obtain the optimum sample thickness.

The extraction of the oscillating EXAFS function $\chi(k)$ from the fluorescence excitation spectra $\mu(E) = I_f/I_0$ (here E is the X-ray photon energy) was carried out in the traditional way [30,31]. After subtracting the background below the absorption edge, the monotonic part $\mu_0(E)$ of the spectrum was approximated with splines, and the dependence $\chi = (\mu - \mu_0)/\mu_0$ was calculated as a function of the photoelectron wave vector $k = (2m(E - E_0)/\hbar^2)^{1/2}$. The energy corresponding to the inflection point on the $\mu(E)$ curve was taken as the photoelectron energy origin E_0. The EXAFS spectra were processed with a widely used IFEFFIT software package [32] similarly to [21,33]. For each sample, 3–4 spectra were recorded, they were then independently processed, and the obtained $\chi(k)$ curves were averaged. Details of data processing are given in Ref. [31].

The geometry, electronic structure, and magnetic moment of impurity centers were calculated from first principles using the ABINIT software package in the LDA+U approximation. To correctly describe Fe atoms with a partially filled d shell, we used the PAW pseudopotentials [34]. The parameters describing the Coulomb and exchange interactions for the impurity atom were $U = 5$ eV and $J = 0.9$ eV. As shown in our earlier studies [35], in order to obtain relatively narrow impurity bands in the energy spectrum, it is necessary to use supercells containing more than 40 atoms. Therefore, to simulate isolated impurity

Local environment of Fe ions in different models

Model	S	Shell						
		1	2	3	4	5	6	7
Off-center Fe^{2+} ion at the *A* site, displacement [100]	2	2.027 (4O)	2.963 (4Ti)	3.048 (1Sr)	3.170 (4O)	3.633 (4O)	3.818 (4O)	4.021 (4Ti)
Off-center Fe^{2+} ion at the *A* site, displacement [110]	2	2.104 (4O)	2.156 (1O)	2.815 (2Ti)	3.195 (2O)	3.377 (2Sr)	3.434 (4O)	3.437 (4Ti)
Off-center Fe^{2+} ion at the *A* site, displacement [111]	2	2.013 (3O)	2.607 (1Ti)	2.936 (6O)	3.233 (3Ti)	3.514 (3Sr)	3.642 (3O)	3.708 (3Ti)
Isolated Fe^{3+} ion at the *B* site (compensated by Y)	5/2	1.988 (6O)	3.374 (7Sr)	3.904 (6Ti)	4.368 (24O)	5.521 (12Ti)		
Fe^{3+}-V_O complex (compensated by Sc)	5/2	1.902 (1O)	1.964 (4O)	3.416 (4Sr)	3.499 (4Sr)	3.702 (1Ti)	3.926 (4Ti)	4.149 (1Ti)
Isolated Fe^{4+} ion at the *B* site	2	1.932 (6O)	3.360 (8Sr)	3.890 (6Ti)	4.358 (24O)	5.515 (12Ti)		

centers, we used 80-atom FCC supercells in which one of Ti^{4+} ions at the *B* site or Sr^{2+} ions at the *A* site was replaced by an impurity atom. The cutoff energy of plane waves in the calculations was 30 Ha (816 eV), and the integration over the Brillouin zone was carried out on the $2\sqrt{3} \times 2\sqrt{3} \times 2\sqrt{3}$ Monkhorst–Pack mesh. The relaxation of the lattice parameters and atomic positions was carried out until the forces acting on the atoms became less than 10^{-5} Ha/Bohr (0.5 meV/Å). When a change in the oxidation state of iron was necessary, oxygen vacancies as well as donor or acceptor impurities located at the maximum distance from the impurity atom were added to the structure.

3. Results of first-principles calculations

For reliable identification of defects in $SrTiO_3$(Fe) samples by EXAFS spectroscopy, we need structural models of possible defects. For this purpose, calculations of the local environment, electronic structure, and magnetic moment of several iron-containing complexes were carried out. According to the literature, in bulk $SrTiO_3$ samples, in addition to iron atoms at the *B* sites in the +4 oxidation state, a certain fraction of Fe atoms at these sites can be in the +3 oxidation state both as isolated ions and complexes with oxygen vacancies. Therefore, we need to study the structure of possible complexes of Fe with oxygen vacancies. For atoms at the *A* site, the supposed oxidation state is +2. Such doping does not violate the electrical neutrality of the samples, and it is sufficient to consider only point defects (isolated impurity atoms) in them. The results of calculations of the local environment and magnetic moments of the ions are given in Table.

Calculations for an isolated Fe^{3+} ion at the *B* site, for which a donor Y atom at the Sr site was added to the supercell to obtain the required oxidation state, showed that the energetically most favorable state of the ion is the high-spin state with a magnetic moment of $5\mu_B$. In the case of the Fe^{3+}-V_O complex with the nearest oxygen vacancy and a compensating acceptor impurity Sc_{Ti}, the magnetic moment of the ion is also $5\mu_B$. For an isolated Fe^{4+} ion, the magnetic moment is $4\mu_B$.

For the Fe^{2+} ion at the *A* site, the on-center position of the impurity atom turned out to be unstable. That is why we calculated three configurations corresponding to possible off-center displacements of this atom along the [100], [110], and [111] directions. The values of the corresponding off-center displacements were 1.14, 0.96, and 0.95 Å. In all three configurations, the Fe ion is in a high-spin state (magnetic moment $4\mu_B$).

In the obtained results, attention should be drawn to the fact that the Fe–O interatomic distances for off-center atoms at the *A* site are close to the Fe–O distances for the *B* site (Table). This can strongly complicate the analysis of the EXAFS spectra.

4. Results and discussion

4.1. X-ray diffraction

In what follows, to designate the samples we will use names consisting of a number — the nominal concentration of the impurity in percent, a letter — a site into which the impurity should enter, and numbers — the annealing temperature (for example, 2A1500 means the $Sr_{0.98}Fe_{0.02}TiO_3$ sample annealed at 1500°C).

X-ray studies of $SrTiO_3$(Fe) samples showed that all samples have a cubic perovskite structure at 300 K (Fig. 1). Among the studied samples, only one sample turned out to be single-phase — the 3B1500 sample. The diffraction patterns of the samples annealed at 1100°C clearly showed the lines of TiO_2 and of the Ruddlesden–Popper $Sr_3Ti_2O_7$

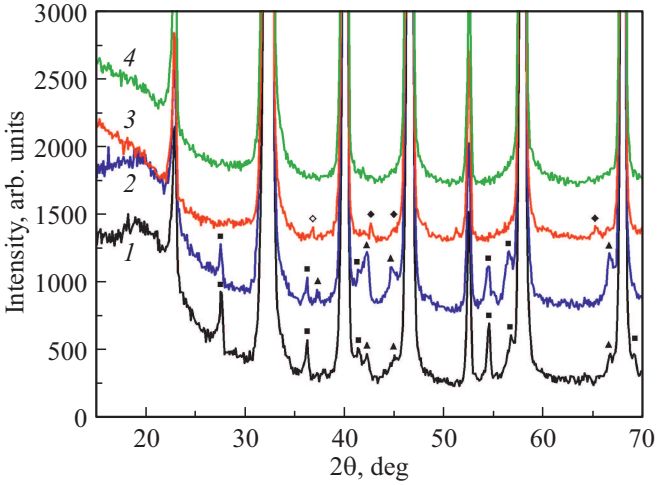

Figure 1. X-ray diffraction patterns of $SrTiO_3$(Fe) samples: (*1*) 2A1100, (*2*) 3B1100, (*3*) 2A1500, and (*4*) 3B1500. The squares denote the reflexes of the TiO_2 second phase, and the triangles denote the position of the lines of the $Sr_3Ti_2O_7$ Ruddlesden–Popper phase. The filled diamonds mark the $Sr_3Fe_2O_7$ lines, and an open diamond indicates the line of the Fe_2TiO_5 phase.

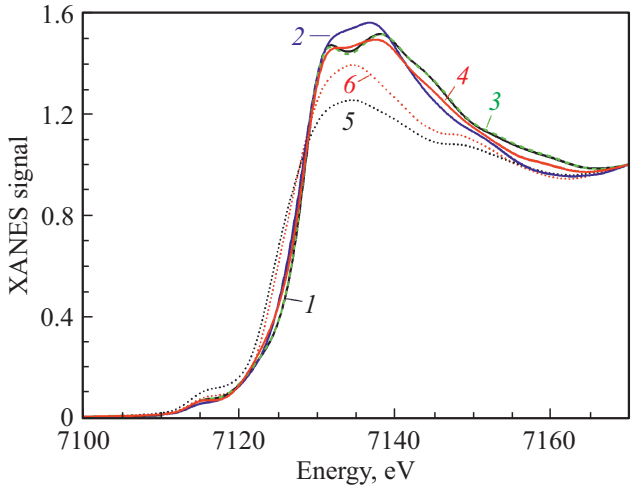

Figure 2. XANES spectra of $SrTiO_3$(Fe) samples and reference compounds: (*1*) 2A1100, (*2*) 2A1500, (*3*) 3B1100, (*4*) 3B1500, (*5*) $FeTiO_3$, (*6*) Fe_2O_3.

phase, whose concentrations, however, were not high. The appearance of the Ruddlesden–Popper phase, which contains an excess of strontium, compensates for the segregation of titanium in the form of TiO_2. The ratio of intensities of the corresponding lines is consistent with the deviation from stoichiometry created in the samples. The diffraction pattern of the 2A1500 sample showed weak lines, three of which can be identified as the Ruddlesden–Popper phase $Sr_3Fe_2O_7$, and the line at $2\theta = 36.75°$ — as the precipitation of Fe_2TiO_5. The line at $2\theta = 51.3°$ remains unidentified. A very small amount of the second phase in the 2A1500 sample may indicate successful incorporation of the iron atoms into the *A* sites.

4.2. XANES Spectra

To determine the oxidation state of the Fe impurities in $SrTiO_3$, the position of the absorption edges in the XANES spectra of the $SrTiO_3$(Fe) samples was compared with the position of the absorption edges in the $FeTiO_3$ and Fe_2O_3 reference compounds (Fig. 2). Unfortunately, the above method for determining the oxidation state was not very successful. The shift of the absorption edge between the reference samples of divalent and trivalent Fe as well as between the samples obtained under different preparation conditions, was only ~ 0.5 eV. This was insufficient for reliable identification of the impurity oxidation state. The weak influence of the ionic charge on the position of the Fe *K*-edge was also noticed in Ref. [26].

It is noteworthy that the shape of the XANES spectra of both samples annealed at 1500°C in the energy range 7131–7142 eV differs from that of the samples annealed at 1100°C. In our opinion, this may indicate a change in the position of the impurity and the incorporation of some iron atoms into the *A* sites.

4.3. EXAFS Spectra

To determine the structural position of the Fe impurities in $SrTiO_3$, we analyzed the EXAFS spectra. When analyzing the data, we took into account the lattice parameter obtained from the X-ray measurements, and, when choosing the structural models, the results of calculations of the defects' geometries which included all relaxations of the surrounding atoms (Sec. 3). In addition, the possibility of the impurity atoms to enter both the *A* and *B* sites of the perovskite structure was considered [21,22].

The results of processing of the experimental EXAFS data of $SrTiO_3$(Fe) samples and their best fits using different theoretical models are shown in Fig. 3. The used models were the model with the Fe atom at the *B* site and the model with the simultaneous incorporation of the impurity into the *B* and *A* sites. In the latter case, the atom at the *A* site was assumed to be off-center.

An analysis of the EXAFS data showed the following. In the EXAFS region, regardless of the preparation conditions, the spectra were qualitatively described by a model in which the Fe atom replaces the atom at the *B* site with the interatomic Fe–O distances varying from 1.906 Å for the 3B1100 sample to 1.930 Å for the 3B1500 sample, and to 1.949 Å for the 2A1500 sample. Taking into account the results obtained in Ref. [26], we suggest that the iron atoms are predominantly in the +4 oxidation state in samples annealed at 1100°C, and in the +3 and +4 oxidation states in samples annealed at 1500°C. The obtained interatomic distances agree with the results of first-principles calculations (Table). However, the difference in interatomic distances in the samples, which were annealed at the

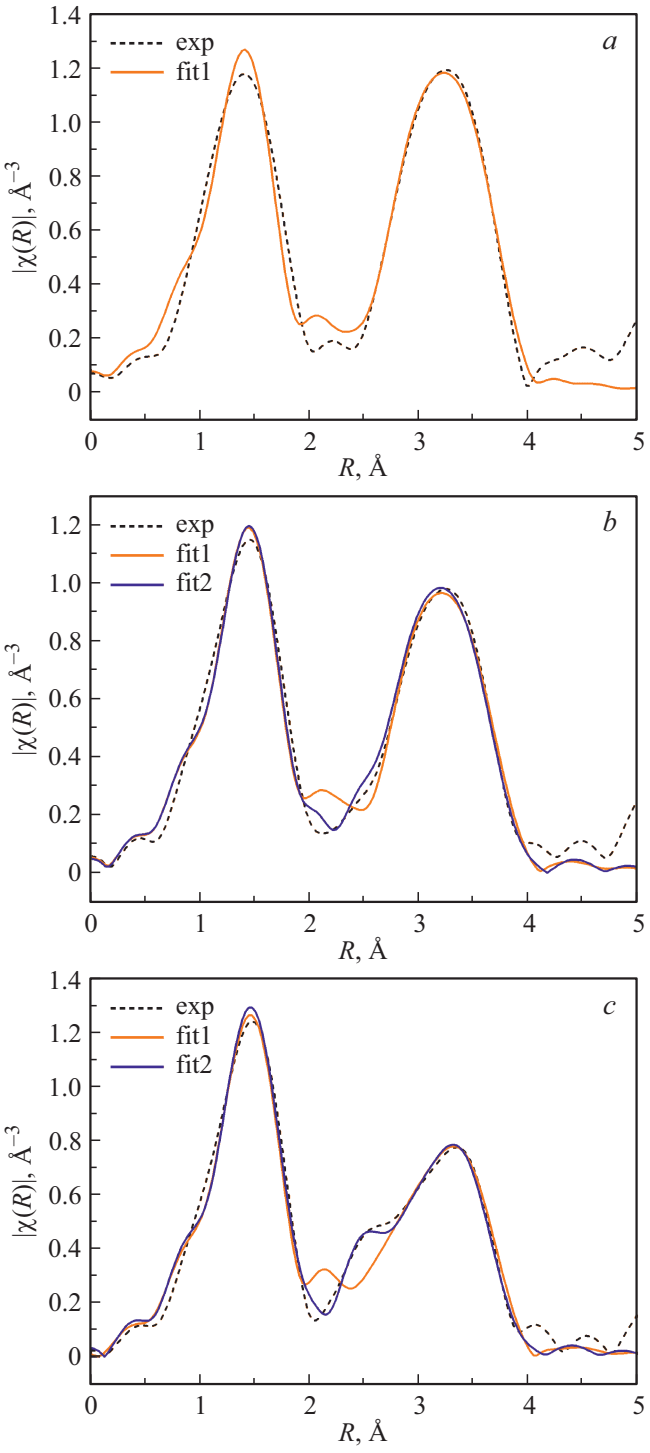

Figure 3. Fourier transforms of experimental EXAFS spectra in the *R*-representation (exp) and their best fits in the model with Fe atoms only at the *B* sites (fit1) and the model with the simultaneous presence of iron at the *A* and *B* sites (fit2).

same temperature (1500°C) but had different deviation from stoichiometry, when taking into account the results of calculations in Sec. 3, enable us to suppose that a part of the iron atoms enter the *A* site since the average Fe–O distance for the *A* site is bigger than for the *B* site.

As follows from Fig. 3, the EXAFS spectra of the samples annealed at 1500°C having different deviation from stoichiometry are qualitatively different. The deviation of the curves is especially noticeable in the range 1.9–2.9 Å, in which additional features associated with a change in the local environment should appear when the impurity atoms enter the *A* site (Table). In order to test this hypothesis, we analyzed the EXAFS spectra using a model of simultaneous incorporation of Fe into both lattice sites, assuming that the direction of the off-center displacement of the atom is [100]. For this model, the agreement of the spectra has indeed noticeably improved (Fig. 3).

The strongest contributions to the EXAFS spectra from the Fe atom at the *A* site come from the nearest O and Ti atoms. From the comparison of the Fe–Ti distance of 2.99 Å obtained from the EXAFS data analysis with the distances calculated for different off-centering models (Table) it follows that the most probable direction of the displacement of Fe atom from the *A* site is indeed the [100] one.

According to our data, the fraction of the Fe atoms at the *A* sites increased from ~ 0.24 in the 3B1500 sample to ~ 0.31 in the 2A1500 sample. It is interesting that according to our results, at a high annealing temperature some Fe atoms enter the *A* sites even for deviation from stoichiometry toward strontium. We believe that small precipitates of the second phase observed in the X-ray diffraction of the 2A1500 sample cannot be the cause of such noticeable changes in the EXAFS spectra.

The overestimated Debye–Waller factors for the nearest oxygen atoms in our samples (0.008 $Å^2$) are in good agreement with the data for oxidized samples obtained in Ref. [27]. In that work, this overestimation was explained by the Jahn–Teller distortion around the Fe^{4+} ion. However, our results admit another explanation — the coexistence of two structural positions of the iron atoms, which slightly differ in the Fe–O distance.

The low concentration of iron at the *A* site and the closeness of the Fe–O distances in models with the atoms at *A* and *B* sites did not enable us to more accurately determine the parameters of structural models. To solve this problem, it is desirable to synthesize samples with a higher fraction of iron at the *A* site (for example, by synthesizing samples at higher annealing temperatures and, possibly, in a reducing atmosphere) and to measure the EXAFS spectra at lower temperatures.

5. Conclusion

In this work, an attempt has been undertaken to incorporate the iron impurity into the *A* sites of strontium titanate. The results obtained from the analysis of X-ray diffraction, XANES spectra, and EXAFS spectra give substantial grounds to suppose that at a high annealing temperature the Fe atoms enter, at least partially, the *A* sites. For more reliable identification of iron at the *A* site, it is

desirable to study samples with a higher fraction of the atoms at the *A* site and to analyze the EXAFS spectra obtained at a lower temperature. According to our data, the Fe impurity in $SrTiO_3$ exhibits a strong off-centering at the *A* site (the displacement of ~ 1 Å) similar to that previously established for strontium titanate doped with Mn and Co. This explains the cause of dielectric relaxations in $SrTiO_3$(Fe) samples observed in Ref. [23].

Acknowledgments

The authors express their gratitude to BESSY for the opportunity to carry out our experiments and financial support of this project.

Conflict of interest

The authors declare that they have no conflict of interest.

References

[1] Properties and applications of perovskite-type oxides. / Ed. L.G. Tejuca, J.L.G. Fierro. CRC Press, N.Y. (1993).
[2] H.-C. Li, W. Si, A.D. West, X.X. Xi. Appl. Phys. Lett. **73**, *2*, 190 (1998).
[3] K. Eisenbeiser, J.M. Finder, Z. Yu, J. Ramdani, J.A. Curless, J.A. Hallmark, R. Droopad, W.J. Ooms, L. Salem, S. Bradshaw, C.D. Overgaard. Appl. Phys. Lett. **76**, *10*, 1324 (2000).
[4] J. Li, S. Li, F. Liu, M.A. Alim, G. Chen. J. Mater. Sci.: Mater. Electron. **14**, *8*, 483 (2003).
[5] S. Ohta, T. Nomura, H. Ohta, M. Hirano, H. Hosono, K. Koumoto. Appl. Phys. Lett. **87**, *9*, 092108 (2005).
[6] X. Lin, G. Bridoux, A. Gourgout, G. Seyfarth, S. Krämer, M. Nardone, B. Fauqué, K. Behnia. Phys. Rev. Lett. **112**, *20*, 207002 (2014).
[7] J. Park, D.-H. Kwon, H. Park, C.U. Jung, M. Kim. Appl. Phys. Lett. **105**, *18*, 183103 (2014).
[8] H. Kato, A. Kudo. J. Phys. Chem. B **106**, *19*, 5029 (2002).
[9] R. Konta, T. Ishii, H. Kato, A. Kudo. J. Phys. Chem. B **108**, *26*, 8992 (2004).
[10] T. Hara, T. Ishiguro. Sens. Actuators B **136**, *2*, 489 (2009).
[11] V.V. Lemanov, E.P. Smirnova, A.V. Sotnikov, M. Weihnacht, Phys. Solid State **46**, *8*, 1442 (2004).
[12] V.V. Lemanov, A.V. Sotnikov, E.P. Smirnova, M. Weihnacht. J. Appl. Phys. **98**, *5*, 056102 (2005).
[13] A. Tkach, P.M. Vilarinho, A.L. Kholkin. Appl. Phys. Lett. **86**, *17*, 172902 (2005).
[14] A.I. Lebedev, I.A. Sluchinskaya, A. Erko, V.F. Kozlovskii, JETP Lett. **89**, *9*, 457 (2009).
[15] I. Levin, V. Krayzman, J.C. Woicik, A. Tkach, P.M. Vilarinho. Appl. Phys. Lett. **96**, *5*, 052904 (2010).
[16] I.A. Sluchinskaya, A.I. Lebedev, A. Erko, Bull. Russ. Acad. Sci.: Phys. **74**, *9*, 1235 (2010).
[17] M. Valant, T. Kolodiazhnyi, I. Arcon, F. Aguesse, A.-K. Axelsson, N.M. Alford. Adv. Funct. Mater. **22**, *10*, 2114 (2012).
[18] R.A. Maier, E. Cockayne, M. Donohue, G. Cibin, I. Levin. Chem. Mater. **32**, *11*, 4651 (2020).
[19] V.V. Shvartsman, S. Bedanta, P. Borisov, W. Kleemann, A. Tkach, P.M. Vilarinho. Phys. Rev. Lett. **101**, *16*, 165704 (2008).
[20] W. Kleemann, V.V. Shvartsman, S. Bedanta, P. Borisov, A. Tkach, P.M. Vilarinho. J. Phys.: Condens. Matter. **20**, *43*, 434216 (2008).
[21] I.A. Sluchinskaya, A.I. Lebedev, Phys. Solid State **61**, *3*, 390 (2019).
[22] I.A. Sluchinskaya, A.I. Lebedev. J. Alloys. Comp. **820**, 153243 (2020).
[23] C. Garg, J. Kumar, S. Nair. Phys. Rev. Mater. **2**, *9*, 094409 (2018).
[24] S. Molin, W. Lewandowska-Iwaniak, B. Kusz, M. Gazda, P. Jasinski. J. Electroceram. **28**, *1*, 80 (2012).
[25] B.W. Faughnan. Phys. Rev. B **4**, *10*, 3623 (1971).
[26] C. Lenser, A. Kalinko, A. Kuzmin, D. Berzins, J. Purans, K. Szot, R. Waser, R. Dittmann. Phys. Chem. Chem. Phys. **13**, *46*, 20779 (2011).
[27] M. Vracar, A. Kuzmin, R. Merkle, J. Purans, E.A. Kotomin, J. Maier, O. Mathon. Phys. Rev. B **76**, *17*, 174107 (2007).
[28] V.E. Alexandrov, J. Maier, R.A. Evarestov. Phys. Rev. B **77**, *7*, 075111 (2008).
[29] A. Koehl, D. Kajewski, J. Kubacki, C. Lenser, R. Dittmann, P. Meuffels, K. Szot, R. Waser, J. Szade. Phys. Chem. Chem. Phys. **15**, *21*, 8311 (2013).
[30] A.I. Lebedev, I.A. Sluchinskaya, V.N. Demin, I.H. Munro, Bull. Russ. Akad. Sci.: Phys. **60**, *10*, 1533 (1996).
[31] A.I. Lebedev, I.A. Sluchinskaya, V.N. Demin, I.H. Munro. Phys. Rev. B **55**, *22*, 14770 (1997).
[32] B. Ravel, M. Newville. J. Synchrotron Rad. **12**, *4*, 537 (2005).
[33] I.A. Sluchinskaya, A.I. Lebedev, Phys. Solid State **59**, *8*, 1512 (2017).
[34] K.F. Garrity, J.W. Bennett, K.M. Rabe, D. Vanderbilt. Comput. Mater. Sci. **81**, 446 (2014).
[35] A.I. Lebedev, I.A. Sluchinskaya. Ferroelectrics **501**, *1*, 1 (2016).